arXiv:1205.3418v1 [nucl-th] 15 May 2012

The systematic study of the influence of neutron excess on the fusion cross sections using different proximity-type potentials

O. N. Ghodsi and R. Gharaei*

Sciences Faculty, Department of Physics, University of Mazandaran
P. O. Box 47415-416, Babolsar, Iran

Abstract

Using different types of proximity potentials, we have examined the trend of variations of barrier characteristics (barrier height and its position) as well as fusion cross sections for 50 isotopic systems including various collisions of C, O, Mg, Si, S, Ca, Ar, Ti and Ni nuclei with $1 \leq N/Z < 1.6$ condition for compound systems. The results of our studies reveal that the relationships between increase of barrier positions and decrease of barrier heights are both linear with increase of N/Z ratio. Moreover, fusion cross sections also enhance linearly with increase of this ratio.

PACS: 24.10.-i, 25.70.-z, 25.60.Pj, 25.70.Jj
Keywords: Nuclear-reaction models and methods, Low and intermediate energy heavy-ion reactions, Fusion reactions, Fusion and fusion-fission reactions

---

*email: r.gharaei@stu.umz.ac.ir

1. INTRODUCTION

In recent years, using the neutron-rich projectiles and the formation of the neutron-rich heavy nuclei, the interesting properties of these fusion reactions have been discovered. In general, the compound nucleus resulting from the fusion of the neutron-rich nuclei is placed far from the β-stability line. Furthermore, increasing the neutrons in the interaction nuclei leads to reduction fusion barrier height. Therefore, fusion cross section increases for neutron-rich projectile nuclei, with respect to nuclei that lying near the stability line [1, 2].

For the first time, R. K. Puri *et al.* performed a systematic study on the isotopic dependence of fusion cross section [3]. They calculated nuclear potential using the Skyrme energy density model (SEDM), which it is quite successful in explaining the fusion of two interaction nuclei at low energies [4-14], for different colliding systems involving ^{A_1}Ca+^{A_2}Ca, ^{A_1}Ca+^{A_2}Ni and ^{A_1}Ni+^{A_2}Ni with $1 \leq N/Z \leq 2$. In this condition, N and Z is neutron and proton numbers of compound nucleus in each reaction. According to Ref. [3], with increasing neutron in each group of these colliding systems, the barrier heights V_B decrease and the fusion cross sections σ_{fus} increase. Moreover, the variations of R_B, V_B and σ_{fus} with increasing ratio (N/Z) are linear (see Eqs. (11), (12) and (15) of Ref. [3]).

Recently, R. K. Puri and N. K. Dhiman have also carried out two systematic studies on the isotopic dependence of fusion probabilities using SEDM and several different theoretical models such as parameterized potentials due to Christensen and Winther, Ngô and Ngô and etc. Their investigations is consist of two ranges of different isotopes collision of Ca and Ni nuclei with $0.6 \leq N/Z \leq 1$ [15] and Ca, Ni, Ti and Ni nuclei with $0.5 \leq N/Z \leq 1$ [16]. Their results show that the variations of heights and positions of barrier are non-linear (second order), whereas the fusion cross sections vary as linear with increasing ratio of N/Z for colliding different systems (for example, see Eqs. (11) and (12) of Ref. [15]). The study of neutron rich nuclei is also reported at heavy-ion collisions with intermediate energies. The effects of isospin degree of freedom in collective and elliptic flow have been studied, for example, in Refs. [17-20].

In this paper, we have performed a systematic study on the relationships between variations of heights and positions of barrier and fusion cross sections with increasing N/Z ratio by using the different proximity-type potentials, which shall be introduced in the following section. We have selected thirteen groups of isotopic systems, namely ^{A_1}C+^{A_2}Si, ^{A_1}O+^{A_2}Mg, ^{A_1}O+^{A_2}Si, ^{A_1}Si+^{A_2}Si, ^{A_1}Mg+^{A_2}S, ^{A_1}Si+^{A_2}Ni, ^{A_1}Ca+^{A_2}Ca, ^{A_1}S+^{A_2}Ni, ^{A_1}Ar+^{A_2}Ni, ^{A_1}Ca+^{A_2}Ni, ^{A_1}Ni+^{A_2}Ni, ^{A_1}Ti+^{A_2}Ni and ^{A_1}Ca+^{A_2}Ti with $1 \leq N/Z < 1.6$. In all these systems, the empirical data have been reported (see Table 1). In this work, we follow the procedure proposed in Ref. [3].

2. THE PROXIMITY FORMALISM

The interaction potential between target and projectile nuclei is one of the most important factors in the description of the fusion reaction. In general, this potential consists of two parts, short-range nuclear attraction $V_N(r)$ and large-range coulomb repulsion $V_C(r)$. Proximity model is one of the practical types in calculation of nuclear potential. When two surfaces are approaching each other, approximately in distance of 2-3 fm, an additional force due to the proximity of the surface will appear which is called as proximity potential. All versions of this model are based on the proximity force theorem [21]. According to this theory, nuclear part of total interaction potential is product of a factor depending on the mean curvature of the interaction surface and a universal function depending on the separation distance. Furthermore, nuclear potentials in the proximity formalism are independent of the masses of interaction nuclei. Using the proximity potentials dependence on the liquid drop model, one expects that the nuclear matter incompressibility is one of the intrinsic properties in this formalism.

12 different versions of the proximity model have been introduced by R. K. Puri *et al.* in Ref. [22]. Their investigations show that all proximity potentials are able to reproduce experimental data within 10%, on the average. Among various potentials in Ref. [22], the Aage Winther (AW 95) [23], Bass 1980 (Bass 80) [24] and Denisov Potential [25] (Denisov DP, which in this paper we have used as Prox. DP) have the best agreement with the experimental data. Therefore, in first step, we have selected these versions for calculating the nuclear potential. In addition to above potentials, we have used the Proximity 2010 (Prox. 2010) potential [26] for study of the isotopic dependence in all thirteen mentioned systems. In the following subsections, we have briefly introduced these versions of proximity potential.

A. Aage Winther (AW 95)

Aage Winther, in 1995, introduced a form of nuclear potential by taking Woods-Saxon parametrization as [23],

$$V_N(r) = -\frac{V_0}{1+\exp(\frac{r-R_1-R_2}{a})}, \tag{1}$$

with

$$V_0 = 16\pi\frac{R_1 R_2}{R_1+R_2}\gamma a, \tag{2}$$

here surface energy coefficient γ has the following form

$$\gamma = 0.95\Big[1-1.8\Big(\frac{N_P-Z_P}{A_P}\Big)\Big(\frac{N_T-Z_T}{A_T}\Big)\Big]. \tag{3}$$

Winther adjusted the diffuseness a and radius R_i parameters through a wide comparison with experimental data for heavy-ion elastic scattering. This refined adjustment leads to a new form of a and R_i parameters, which have been defined by Eqs. (8) and (9) of Ref. [23].

B. Bass 1980 (Bass 80)

Bass in 1977 [27] and 1980 [28] introduced a nucleus-nucleus potential which is labeled as Bass 80. This potential has been derived from the liquid drop model and geometric interpretation of the fusion data in the above regions of the barrier for systems with $Z_P Z_T = 64 - 850$. In this model the nuclear part of the interaction potential can be written as [24],

$$V_N(r) = \frac{R_1 R_2}{R_1 + R_2}\Phi(s), \tag{4}$$

where $s = r - R_1 - R_2$. Here the universal function $\Phi(s)$ has the following form,

$$\Phi(s) = \left[0.033\mathrm{exp}(\frac{s}{3.5}) + 0.007\mathrm{exp}(\frac{s}{0.65})\right]^{-1} \tag{5}$$

with central radius, R_i, as

$$R_i = R_s\left(1 - \frac{0.98}{R_s^2}\right) \qquad (i = 1, 2) \tag{6}$$

where the sharp radii R_s has been defined by using the Eq. (4) of Ref. [22].

C. Denisov DP (Prox. DP)

Denisov, using the semi-microscopic approximation and examination of 119 spherical or near spherical even-even nuclei around the β-stability line, has defined an expression for nuclear part of total interaction potential as the following form [25],

$$V_N(r) = -1.989843\overline{R}\Phi(s) \times \left[1 + 0.003525139(\frac{A_1}{A_2} + \frac{A_2}{A_1})^{3/2} - 0.4113263(I_1 + I_2)\right]. \tag{7}$$

where $s = r - R_1 - R_2 - 2.65$ and $\overline{R} = R_1 R_2/(R_1 + R_2)$. The explicit form of the universal function $\Phi(s)$ and effective nuclear radius R_i have been defined by Eqs. (11), (12) and (13) of Ref. [25].

D. Proximity 2010 (Prox. 2010)

The effect of surface energy coefficient γ in the proximity potential, has been discussed in Ref. [26]. In this study, four different versions of surface energy coefficient γ have been introduced based on the Prox. 77 potential [21]. The obtained results show that the barrier heights and positions as well as fusion cross sections due to Prox. 77 potential with new surface energy coefficient, namely γ-MN1976, have the best agreement with experimental data (see Figs. (3) and (4) of Ref. [26]). This modified proximity potential is labeled as proximity 2010. In this model, the nuclear potential $V_N(r)$ has the following form,

$$V_N(r) = 4\pi\overline{R}\gamma\Phi(r - C_1 - C_2), \tag{8}$$

with

$$\gamma = \gamma_0\Big[1 - K_s\Big(\frac{N - Z}{A}\Big)^2\Big]. \tag{9}$$

Among different values for constants γ_0 and K_s, the set of $\gamma_0 = 1.460734$ MeV/fm^2 and $K_s = 4.0$ have the best results for barrier heights and fusion cross sections in the many systems that have been evaluated in Ref. [26]. In Eq. (8), $\overline{R}$ is the reduced radius and C$_1$ (or C$_2$) is known as Süssmanns centarl radius. The explicit form of these parameters as given by Eqs. (2) and (3) of Ref. [22]. The universal function $\Phi(r - C_1 - C_2)$ has been defined by Eq. (6) of Ref. [22].

3. CALCULATIONS

In order to calculate the nuclear potential, we have employed four versions of the proximity model, *i.e.* AW 95, Bass 80, Prox. DP and Prox. 2010 potentials. By adding the Coulomb potential to a nuclear part, we get the total potential $V_T(r)$ as,

$$V_{tot}(r) = V_C(r) + V_N(r), \tag{10}$$

where $V_C(r) = Z_1Z_2e^2/r$. On the other hand, one can determine the barrier position R_B and height V_B by the following conditions,

$$\Big(\frac{dV_{tot}(r)}{dr}\Big)_{r=R_B} = 0 \qquad ; \qquad \Big(\frac{d^2V_{tot}(r)}{dr^2}\Big)_{r=R_B} \leq 0 \tag{11}$$

The calculated values of the R_B and V_B resulting from the AW 95, Bass 80, Prox. DP and Prox. 2010 potentials have been listed in Table 1-4. In these tables, the values of the Coulomb $V_C(r)$ and nuclear $V_N(r)$ potentials in $r = R_B$ have also been listed for each reaction. As a result from this calculations, positions and heights of barrier, respectively, increase and decrease with addition of neutron in different colliding systems. The experimental data for barrier heights and fusion cross sections are available for systems with nuclei that are little far from the stability line. However, using the proposed semi-empirical approach in Ref. [29], one can calculate the cross sections for fusion reactions, but doing this work requires the independent calculations which we will employe it as a useful approach in the further investigations. Although, all considered potentials are already applied to more than 400 reactions and compared with data [22, 26], in Fig. 1, the ratio of experimental and calculated values of barrier height and position as a function of $(N/Z - 1)$ for different versions of proximity potentials are plotted. These values, for example, have been calculated for ^{40}Ca+^{40,48}Ca, ^{40}Ca+^{58,62}Ni, ^{28}Si+^{28,30}Si, ^{30}Si+^{28}Si, ^{58}Ni+^{58,64}Ni, ^{64}Ni+^{64}Ni, ^{24}Mg+^{32,34}S and ^{26}Mg+^{32,34}S systems. As can be seen from Fig. 1, our results for R_B and V_B are in good agreement with experimental data for all proximity versions.

For systematic study of the variations of R_B and V_B, the percentage difference of the heights and positions of the fusion barrier with respect to their corresponding values for the N=Z cases defined as,

$$\Delta R_B(\%) = \frac{R_B - R_B^0}{R_B^0} \times 100, \tag{12}$$

$$\Delta V_B(\%) = \frac{V_B - V_B^0}{V_B^0} \times 100, \tag{13}$$

where R_B^0 and V_B^0 are the positions and heights of the barrier for the $N = Z$ cases (As earlier stated, $N = N_1 + N_2$ and $Z = Z_1 + Z_2$; N_i and Z_i are the neutron and proton numbers of two interaction nuclei, respectively). In all systems, where the values of R_B^0 and V_B^0 are not available, a straight-line interpolation is used between the known points to compute the $\Delta R_B(\%)$ and $\Delta V_B(\%)$. The obtained results for percentage difference of R_B and V_B for all selected versions of proximity potential, are plotted in Fig. 2. The results of other investigations have also been displayed in this figure, which show good agreement with our obtained results. As one can see in Fig. 2, the increase of barrier positions and decrease of barrier heights are both linear. We have parameterized these processes by following relations,

$$\Delta R_B(\%) = \alpha\Big(\frac{N}{Z} - 1\Big), \tag{14}$$

$$\Delta V_B(\%) = \beta\Big(\frac{N}{Z} - 1\Big), \tag{15}$$

whose the values of the constants α and β for AW 95, Bass 80, Prox. DP, and Prox. 2010 potentials have been listed in Table 5. We expect that with increase of neutron in the interaction nuclei of thirteen groups of colliding systems, the nuclear attractive force increases and therefore the heights of barrier decrease (see Fig. 2). To display the increase of nuclear potential with addition of neutron, like Eqs. (14) and (15), we have parameterized the trend of V_N variations. The obtained results have been shown in Fig. 3. As one can see from this figure, the nuclear potential, like height and position of barrier, increase linearly. This process has been parameterized by following relations,

$$\Delta V_N(\%) = \gamma\Big(\frac{N}{Z} - 1\Big), \tag{16}$$

whose the values of the constants γ for our selected potentials have also been listed in Table 5.

One can also examine this phenomenon by a different approach. According to the Pauli exclusion principle, which prevent the overlapping of the wave functions of two systems of fermions, we expect the interaction potential between two colliding nuclei will contain an additional repulsive interaction. In nuclear fusion process, when two interaction nuclei complete overlap the nuclear matter density is twice that of the saturation case, $\rho \approx 2\rho_0$. This conduct of density distributions have been displayed, for example, for ^{40}Ca + ^{40}Ca fusion reaction in Fig. 4. In this figure, the solid curves are based on the density distributions of the target and projectile nuclei, whereas the short-dashed curves are based on the total density distribution. It is clear from Fig. 4(c) that the total density at complete overlap of interaction nuclei almost becomes twice its initial value.

According to the nuclear equation of state, where energy per nucleon is proportional to density, increasing density in the overlapping region of two interacting nuclei leads to an increase in the energy of the compound system. This increase of the energy can be attributed to the short-range repulsive interaction in the nuclear part of total interaction potential. By modeling the repulsive core effects [30], shallow packet appears in the inner part of the barrier (see, for example, Fig. 2 of Ref. [30]). The effect of nuclear matter incompressibility on the inner regions of the fusion barrier and the depth of pocket is essential. As a result, a soft nuclear matter provides a deep pocket , whereas a hard one provides a shallow pocket. With the addition of neutrons in each of the thirteen interaction systems, we expect that the nuclear matter increases in the overlap region of the density distributions. This phenomenon leads to an increase of energy and consequently increase of repulsive force resulting from nuclear matter incompressibility effects. This additional repulsive force increases the barrier height and reduces the potential depth.

In Fig. 5, for example, we have shown the total interaction potential by using the two versions of proximity potential, AW 95 and Prox. DP, for ^{A_1}Ni+^{A_2}Ni system. As can be seen in Fig. 5, with increasing neutron in fusion reactions, the pocket energy V_{pocket} is reduced. Therefore, it is predictable that the increase of attractive force could be dominate the increase of the repulsive force.

One-dimensional barrier penetration is one of the applied models for calculation of the fusion cross section. In this formalism, the fusion cross section is given by,

$$\sigma_{fus} = \frac{\pi\hbar^2}{2\mu E_{c.m.}} \sum_{l=0}^{l_{max}} (2l+1) T_l(E_{c.m.}) \tag{17}$$

where $T_l(E_{c.m.})$ is the quantum-mechanical transmission probability through the potential barrier for the *l-th* partial wave and μ is reduced mass of the target and projectile system. With assumption that the width and position of the barrier are independent of angular momentum l and with $E_{c.m.} \gg V_B$, the Eq. (17) is reduced to sharp cutoff formula,

$$\sigma_{fus}(mb) = 10\pi R_B^2 \Big(1 - \frac{V_B}{E_{c.m.}}\Big). \tag{18}$$

In Fig. 6, we have displayed the fusion cross sections, Eq. (18), for ^{40}Ca+^{58,60,62}Ni systems using all four proximity potentials. In this figure, the dashed, short-dashed and dash-dotted curves based on the calculated fusion cross sections for ^{40}Ca+^{58}Ni, ^{40}Ca+^{60}Ni and ^{40}Ca+^{62}Ni, respectively. One observes that the obtained results have a good agreement with experimental data [31], in above barrier. Moreover, with addition of neutron in these fusion reactions, the fusion probabilities are increased.

The percentage difference for fusion cross section is given by the following relation,

$$\Delta\sigma_{fus}(\%) = \frac{\sigma_{fus}(E^0_{c.m.}) - \sigma^0_{fus}(E^0_{c.m.})}{\sigma^0_{fus}(E^0_{c.m.})} \times 100, \tag{19}$$

where $E^{0}_{c.m.} = E_{c.m.}/V^{0}_{B}$. According to the condition $E_{c.m.} \gg V_B$, we have calculated this percentage difference for two center-of-mass energies $E_{c.m.} = 1.125V^{0}_{B}$ and $E_{c.m.} = 1.375V^{0}_{B}$, for example. The obtained results for AW 95, Bass 80, Prox. DP, and Prox. 2010 potentials have been shown in Fig. 7. As see from this figure, the relationship between changes of the fusion cross sections with increasing neutron (or ratio N/Z) in four versions of potential are linear. This relation is given by,

$$\Delta\sigma_{fus}(\%) = c\Big(\frac{N}{Z} - 1\Big), \tag{20}$$

where the values of constant c for different potentials and energies have been listed in Table 5. In order to reduce the barrier height with increasing neutron, see Table 1-4, one expects an increase of fusion cross section in each of the interaction systems. This phenomenon is well visible in Fig. 7.

4. CONCLUSION

Our purpose in this paper is a systematic study on the neutron excess effect in 50 isotopic reactions ^{A_1}C+^{A_2}Si, ^{A_1}O+^{A_2}Mg, ^{A_1}O+^{A_2}Si, ^{A_1}Si+^{A_2}Si, ^{A_1}Mg+^{A_2}S, ^{A_1}Si+^{A_2}Ni, ^{A_1}Ca+^{A_2}Ca, ^{A_1}S+^{A_2}Ni, ^{A_1}Ar+^{A_2}Ni, ^{A_1}Ca+^{A_2}Ni, ^{A_1}Ni+^{A_2}Ni, ^{A_1}Ti+^{A_2}Ni and ^{A_1}Ca+^{A_2}Ti with $1 \leq N/Z < 1.6$. The nuclear part of total interaction potential has been calculated by using the proximity potentials AW 95, Bass 80, Prox. DP, and Prox. 2010, whose values of heights and positions of the barrier and fusion cross sections in these potentials according to Refs. [22, 26, 32], have the best agreement with experimental data. In this work, the obtained results are included the following cases:

(i) We have found a linear relation between changes of the barrier position ΔR_B and barrier height ΔV_B with increasing of the ratio N/Z in thirteen groups of the fusion reactions (see Eqs. (14) and (15)). (ii) The parametrization of nuclear potential $V_N(r)$ in $r = R_B$ shows that the trend of $V_N(r)$ versus N/Z ratio is linear for all considered potentials. (iii) The changes of the fusion cross sections $\Delta\sigma_{fus}$ with increasing of the ratio N/Z in thirteen groups of the interaction systems are linear (see Eq. (20)). (iv) The reduction the Coulomb barrier height and consequently increase of the fusion cross section has been attributed to increase of the attractive force due to neutron excess. (v) The attractive force resulting from adding neutrons can be overcome on the repulsive force due to the incompressibility effects.

As a further investigation, one can examine the addition of neutron effects using a systematic study based on the dynamic approach. Ning Wang *et al.*, using improved quantum molecular dynamics (QMD) model, have discussed the influence of dynamic corrections in the near coulomb barrier [33]. The values of Coulomb barrier height and the depth of the mean potential well of the compound nuclei have been calculated in fusion ^{40}Ca+^{90},^{96}Zr and ^{48}Ca+^{90}Zr at energies $E_{c.m.} = 95.0$ MeV (below the barrier) and $E_{c.m.} = 107.6$ MeV (above the barrier) (see Table III of Ref. [33]). The obtained results show that dynamic effects decrease height and thickness of barrier. All these problems are very important for further understanding the mechanism of neutron or proton rich nuclei. We are going to study these aspects in future works.

References

[1] K. E. Zyromski, W. Loveland, G. A. Souliotis, D. J. Morrissey, C. F. Powell, O. Batenkov, K. Aleklett, R. Yanez, I. Forsberg, M. Sanchez-Vega, J. R. Dunn, and B. G. Glagola, Phy. Rev. C **55**, R562 (1997).

[2] Z. H. Liu, C. Signorini, Z. C. Li, L. Mueller, Y. H. Pu, F. Soramel, G. Loebner, K. Rudolph, and C. Zotti, Proc. 8^{th} *Int. Conf. on Nuclear Reaction Mechanisms*, Varenna (Italy), June 9-14, 1997-to be published.

[3] R. K. Puri, M. K. Sharma, R. K. Gupta, Eur. Phys. J. A **3**, 277 (1998).

[4] D. M. Brink and N. Rowley, Nucl. Phys. A **219**, 79 (1974).

[5] D. M. Brink and Fl. Stancu, Nucl. Phys. A **243**, 175 (1975).

[6] Fl. Stancu and D. M. Brink, Nucl. Phys. A **270**, 236 (1976).

[7] D. M. Brink and Fl. Stancu, Nucl. Phys. A **299**, 321 (1978).

[8] C. Ngô, B. Tamain, M. Beiner, R. J. Lombard, D. Mas, and H. H. Deubler, Nucl. Phys. A **252**, 237 (1975).

[9] H. Ngô and Ch. Ngô, Nucl. Phys. A **348**, 140 (1980).

[10] K. C. Panda and T. Patra, J. Phys. G: Nucl. Phys. **14**, 1489 (1988).

[11] R. K. Puri and R. K. Gupta, J. Phys. G: Nucl. Part. Phys. **17**, 1933 (1991).

[12] R. K. Puri and R. K. Gupta, Phys. Rev. C **45**, 1837 (1992).

[13] R. K. Puri and R. K. Gupta, Phys. Rev C **51**, 1568 (1995).

[14] M. K. Sharma, R. K. Puri, and R. K. Gupta, Z. Phys. A **359**, 141 (1997).

[15] R. K. Puri and N. K. Dhiman, Eur. Phys. J. A **23**, 429 (2005).

[16] N. K. Dhiman and R. K. Puri, Acta. Phys. Pol. B **37**, 1855 (2006).

[17] S. Gautam, A. D. Sood, R. K. Puri and J. Aichelin, Phys. Rev. C **83**, 034606 (2011).

[18] S. Gautam, A. D. Sood, R. K. Puri and J. Aichelin, Phys. Rev. C **83**, 014603 (2011).

[19] S. Goyal, R. K. Puri, Nucl. Phys. A **853**, 164 (2011).

[20] S. Gautam, R. Chugh , A. D. Sood, R. K. Puri, Ch. Hartnack and J. Aichelin, J. Phys. G: Nucl. Part. Phys. **37**, 085102 (2010).

[21] J. Blocki, J. Randrup, W. J. Swiatecki and C. F. Tsang, Ann. Phys. (NY) **105**, 427 (1977).

[22] I. Dutt and R. K. Puri, Phys. Rev. C **81**, 064609 (2010).

[23] A. Winther, Nucl. Phys. A **594**, 203 (1995).

[24] W. Reisdorf, J. Phys. G: Nucl. Part. Phys. **20**, 1297 (1994).

[25] V. Y. Denisov, Phys. Lett. B **526**, 315 (2002).

[26] I. Dutt and R. K. Puri, Phys. Rev. C **81**, 047601 (2010).

[27] R. Bass, Phys. Rev. Lett. **39**, 265 (1977).

[28] R. Bass, *Lecture Notes in Physics*, 1980, 117 (Berlin: Springer) pp 281-93.

[29] K. Siwek-Wilczynska, I. Skwira-Chalot and J. Wilczynski, International Journal of Modern Physics E, **16**, No. 2 (2007) 483.

[30] S. Misicu and H. Esbensen, Phys. Rev. C **75**, 034606 (2007).

[31] B. Sikora *et al.*, Phys. Rev. C **20**, 2219 (1979).

[32] I. Dutt and R. K. Puri, Phys. Rev. C **81**, 044615 (2010).

[33] N. Wang, Z. Li and X. Wu, Phys. Rev. C **65**, 064608 (2002).

[34] R. K. Puri and R. K. Gupta, Phys. Rev. C **45**, 1837 (1992).

[35] M. Trotta *et al.*, Phys. Rev. C **65**, 011601(R) (2003).

[36] L. C. Vaz, J. M. Alexander and G. R. Satchler, Phys. Rep. **69**, 373 (1981).

[37] S. Gary and C. Volant, Phys. Rev. C **25**, 1877 (1982).

[38] C. M. Jachcinski, D. G. Kovar, R. R. Betts, C. N. Davids, D. F. Geesaman, C. Olmer, M. Paul, S. J. Sanders, and J. L. Yntema, Phys. Rev. C **24**, 2070 (1981).

[39] R. Rascher, W. F. J Miiller, and K. P. Lieb, Phys. Rev. C **20**, 1028 (1979).

[40] D. G. Kovar, D. F. Geesaman, T. H. Braid, Y. Eisen, W. Henning, T. R. Ophel, M. Paul, K. E.Rehm, S. J Sanders, P. Sperr, J. P. Schiffer, S. L. Tabor, S. Vigdor, B. Zeidman, and F.W. Prosser, Jr., Phys. Rev. C **20**, 1305 (1979).

[41] G. M. Berkowitz, P. Braun-Munzinger, J. S. Karp, R. H. Freifelder, J. R. Renner, and H. W. Wilschut, Phys. Rev. C **28**, 667 (1983).

[42] E. F. Aguilera, J. J. Kolata, P. A. DeYoung, and J. J. Vega, Phys. Rev. C **33**, 1961 (1986).

[43] A. M. Stefanini, G. Fortuna, R. Pengo, W. Meczynski, G. Montagnoli, L. Corradi, A. Tivelli, S. Beghini, C. Signorini, S. Lunardi, M. Morando, and F. Soramel, Nucl. Phys. A **456**, 509 (1986).

[44] H. A. Aljuwair, R. J. Ledoux, M. Beckerman, S. B.Gazes, J. Wiggins, E. R. Cosman, R. R. Betts, S. Saini, and O. Hansen, Phys. Rev. C **30**, 1223 (1984).

[45] M. Trotta *et al.*, Phys. Rev. C **65**, 011601(R) (2001).

[46] E. Tomasi, D. Ardouin, J.Barreto, V. Bernard, B.Cauvin, C. Magnago, C. Mazur, C. Ngo, E. Piasecki, and M. Ribrag, Nucl. Phys. A **373**, 341 (1982).

[47] A. A. Sanzogni *et al.*, Phys. Rev. C **57**, 722 (1998).

[48] Q. Haider and F. B.Malik, Phys. Rev. C **26**, 162 (1982).

[49] U. Jahnke, H. H. Rossner, D. Hilscher, and E. Holub, Phys. Rev. Lett. **48**, 17 (1982).

[50] A. M. Vinodkumar *et al.*, Phys. Rev. C **53**, 803 (1996).

[51] N. V. S. V. Prasad *et al.*, Nucl. Phys. A **603**, 176 (1996).

[52] M. Beckerman, M. Salomaa, A. Sperduto, J. D. Molitoris, and A. DiRienzo, Phys. Rev. C **25**, 837 (1982).

FIGURE CAPTIONS

Fig. 1. The ratio of experimental [36-38,41,42,44,52] and calculated values of barrier height and position based on the AW 95, Bass 80, Prox. DP, and Prox. 2010 potentials for the fusion reactions of ^{24}Mg+^{32,34}S, ^{26}Mg+^{32,34}S, ^{28}Si+^{28,30}Si, ^{30}Si+^{28}Si, ^{40}Ca+^{40,48}Ca, ^{40}Ca+^{58,62}Ni, ^{58}Ni+^{58,64}Ni and ^{64}Ni+^{64}Ni, for example, as a function of $N/Z-1$.

Fig. 2. The percentage increase of fusion barrier position R_B (left panels) and percentage decrease of fusion barrier height V_B (right panels) with respect to their corresponding values for $N=Z$ cases, as a function of the ratio N/Z of the compound system for the AW 95, Bass 80, Prox. DP, and Prox. 2010 potentials. The solid line in each graph is the result of the linear fitting to the calculated values of $\Delta R_B(\%)$ and $\Delta V_B(\%)$. The results of other model have also been displayed [16, 34].

Fig. 3. The percentage increase of nuclear potential V_N with respect to its corresponding values for $N=Z$ cases, as a function of the ratio N/Z of the compound system for the AW 95, Bass 80, Prox. DP, and Prox. 2010 potentials. The solid line in each graph is the result of the linear fitting to the calculated values of $\Delta V_N(\%)$.

Fig. 4. The process of density distributions overlap of interaction nuclei for ^{40}Ca+^{40}Ca reaction in (a) $\rho \approx \rho_0$, (b) $\rho_0 < \rho < 2\rho_0$ and (c) $\rho \approx 2\rho_0$, which ρ and ρ_0 are density in the overlapping region and saturation density, respectively. Total density distribution is shown with dotted curve.

Fig. 5. Ion-Ion potentials for ^{A_1}Ni+^{A_2}Ni system based on the (a) AW 95 and (b) Prox. DP potentials . The pocket energy V_{pocket} is also indicated in one reaction.

Fig. 6. The fusion cross sections as a function of center of mass energy for ^{40}Ca+^{58}Ni, ^{40}Ca+^{60}Ni and ^{40}Ca+^{62}Ni based on the (a) AW 95, (b) Bass 80, (c) Prox. DP, and (d) Prox. 2010 potentials. The experimental data is taken from the Ref. [31].

Fig. 7. The percentage increase of fusion cross section σ_{fus} for $E_{c.m.}$=1.125V_B^0 (left panels) and $E_{c.m.}$=1.375V_B^0 (right panels) with respect to their corresponding values for $N=Z$ cases, as a function of the ratio N/Z of the compound system for the (a) AW 95 (b) Bass 80 (c) Prox. DP and (d) Prox. 2010 potentials. The solid line in each graph is the result of the linear fitting to the calculated values of $\Delta\sigma_{fus}(\%)$.

TABLE CAPTIONS

Table 1. The calculated barrier positions R_B and heights V_B for different fusion reactions using AW 95 potential, compared with the empirical data. The nuclear and Coulomb potentials in $r = R_B$ have also been reported. The systems are listed with respect to their increasing Z_1Z_2 values.

Reaction	N/Z	Z_1Z_2	R_B	V_C	V_N	V_B	$R_B^{Emp.}$	$V_B^{Emp.}$	Ref.
^{12}C+^{28}Si	1	84	8.47	14.28	-1.05	13.23	7.42±0.2	12.59±0.3	[37]
^{12}C+^{29}Si	1.05	84	8.53	14.18	-1.03	13.15	8.19	13.46	[36]
^{12}C+^{30}Si	1.1	84	8.58	14.10	-1.03	13.07	8.39	13.20	[36]
^{16}O+^{24}Mg	1	96	8.52	16.22	-1.20	15.02	8.40±0.4	15.90±0.9	[38]
							8.48	16.00	[39]
^{16}O+^{26}Mg	1.1	96	8.65	15.98	-1.17	14.81	8.70±0.4	16.50±0.9	[38]
^{18}O+^{24}Mg	1.1	96	8.70	15.89	-1.15	14.74	7.80±0.3	14.90±0.9	[40]
^{16}O+^{28}Si	1	112	8.66	18.62	-1.36	17.26	7.98	17.23	[39]
^{16}O+^{29}Si	1.045	112	8.72	18.49	-1.34	17.15	9.12	16.30	[36]
^{16}O+^{30}Si	1.090	112	8.77	18.39	-1.33	17.05	9.18	16.12	[36]
^{18}O+^{28}Si	1.090	112	8.83	18.26	-1.32	16.94	8.76	16.90	[36]
^{24}Mg+^{32}S	1	192	9.08	30.45	-2.21	28.24	8.70±0.3	28.10±1.6	[38]
							9.20	27.93	[41]
^{24}Mg+^{34}S	1.071	192	9.18	30.12	-2.18	27.94	9.40	27.38	[41]
^{26}Mg+^{32}S	1.071	192	9.21	30.02	-2.15	27.87	9.36	27.48	[41]
^{26}Mg+^{34}S	1.143	192	9.31	29.70	-2.10	27.60	9.50	27.11	[41]
^{28}Si+^{28}Si	1	196	9.09	31.05	-2.25	28.80	8.94	28.89	[42]
							8.25±0.2	28.95±0.7	[37]
^{28}Si+^{30}Si	1.071	196	9.20	30.68	-2.22	28.46	8.86	29.13	[42]
							8.47±0.2	28.28±0.7	[37]
^{30}Si+^{30}Si	1.143	196	9.31	30.32	-2.17	28.15	9.06	28.54	[42]
^{28}Si+^{58}Ni	1.048	392	9.84	57.37	-4.07	53.30	9.00±0.9	53.80±0.8	[43]
^{28}Si+^{62}Ni	1.143	392	9.98	56.57	-3.94	52.63	9.89	52.89	[43]
^{28}Si+^{64}Ni	1.190	392	10.04	56.23	-3.92	52.31	9.20±1.0	52.40±1.1	[43]
^{30}Si+^{58}Ni	1.095	392	9.96	56.68	-3.95	52.73	8.30±1.1	52.20±1.2	[43]
^{30}Si+^{62}Ni	1.190	392	10.09	55.95	-3.85	52.10	9.70±1.0	52.20±0.9	[43]
^{30}Si+^{64}Ni	1.238	392	10.15	55.61	-3.81	51.80	9.40±0.8	51.20±0.9	[43]

Table 1. (Continued)

Reaction	N/Z	Z_1Z_2	R_B	V_C	V_N	V_B	$R_B^{Emp.}$	$V_B^{Emp.}$	Ref.
^{40}Ca+^{40}Ca	1	400	9.74	59.14	-4.22	54.92	9.50±0.5	50.60±2.8	[40]
							8.80±0.5	52.30±0.5	[44]
							9.10±0.6	55.60±0.8	[46]
^{40}Ca+^{44}Ca	1.1	400	9.91	58.13	-4.12	54.01	8.50±0.5	51.70±1.2	[44]
^{40}Ca+^{48}Ca	1.2	400	10.08	57.14	-3.96	53.18	7.80±0.3	51.30±1.0	[44]
^{48}Ca+^{48}Ca	1.4	400	10.38	55.50	-3.75	51.75	10.38	51.70	[45]
^{40}Ca+^{46}Ti	1.048	440	9.91	63.94	-4.57	59.37	9.92±0.08	58.03±0.73	[47]
^{40}Ca+^{48}Ti	1.095	440	10.00	63.36	-4.44	58.92	9.97±0.07	58.17±0.62	[47]
^{40}Ca+^{50}Ti	1.143	440	10.07	62.92	-4.43	58.49	10.05±0.07	58.71±0.61	[47]
^{32}S+^{58}Ni	1.045	448	9.95	64.84	-4.61	60.23	8.60±0.9	59.80±1.4	[43]
							8.50±0.3	59.50	[48]
^{32}S+^{64}Ni	1.182	448	10.16	63.50	-4.38	59.12	8.80±0.5	58.10±0.7	[43]
^{34}S+^{58}Ni	1.090	448	10.06	64.13	-4.48	59.65	7.50±0.9	58.40±1.4	[43]
^{34}S+^{64}Ni	1.227	448	10.25	62.95	-4.34	58.61	8.90±0.6	57.20±0.6	[43]
^{36}S+^{58}Ni	1.136	448	10.16	63.50	-4.39	59.11	7.50±0.6	58.00±1.1	[43]
^{36}S+^{64}Ni	1.273	448	10.34	62.39	-4.27	58.12	8.80±0.6	56.70±1.0	[43]
^{40}Ar+^{58}Ni	1.130	504	10.24	70.88	-4.96	65.92		65.30±0.5	[49]
^{40}Ar+^{60}Ni	1.174	504	10.31	70.40	-4.86	65.54		65.50±0.6	[49]
^{40}Ar+^{62}Ni	1.217	504	10.37	70.00	-4.82	65.18		65.10±0.6	[49]
^{40}Ar+^{64}Ni	1.260	504	10.43	69.59	-4.77	64.82		63.90±0.5	[49]
^{40}Ca+^{58}Ni	1.042	560	10.15	79.45	-5.65	73.80	10.20	73.36	[36]
^{40}Ca+^{62}Ni	1.125	560	10.29	78.38	-5.48	72.90	10.35	72.30	[36]
^{48}Ti+^{58}Ni	1.12	616	10.4	85.30	-6.00	79.30	9.8±0.3	78.8±0.3	[50]
^{48}Ti+^{60}Ni	1.16	616	10.47	84.73	-5.89	78.84	10.0±0.3	77.3±0.3	[50]
^{48}Ti+^{64}Ni	1.24	616	10.60	83.69	-5.72	77.97	10.2±0.3	76.7±0.3	[50]
^{46}Ti+^{64}Ni	1.2	616	10.52	84.33	-5.84	78.49	9.7±0.2	76.9±0.1	[51]
^{50}Ti+^{60}Ni	1.2	616	10.55	84.09	-5.77	78.32	9.8±0.2	77.1±0.1	[51]
^{58}Ni+^{58}Ni	1.071	784	10.55	107.03	-7.62	99.41	8.30	97.90	[52]
^{58}Ni+^{64}Ni	1.178	784	10.75	105.04	-7.33	97.71	8.20	96.00	[52]
^{64}Ni+^{64}Ni	1.286	784	10.94	103.21	-7.04	96.17	8.60	93.50	[52]

Table 2. The calculated barrier positions R_B and heights V_B for different fusion reactions using Bass 80 potential. The nuclear and Coulomb potentials in $r = R_B$ have also been reported. The systems are listed with respect to their increasing Z_1Z_2 values.

Reaction	N/Z	Z_1Z_2	R_B	V_C	V_N	V_B
^{12}C+^{28}Si	1	84	8.45	14.31	-1.17	13.14
^{12}C+^{29}Si	1.05	84	8.51	14.21	-1.16	13.05
^{12}C+^{30}Si	1.1	84	8.57	14.11	-1.14	12.97
^{16}O+^{24}Mg	1	96	8.50	16.26	-1.33	14.93
^{16}O+^{26}Mg	1.1	96	8.65	15.98	-1.26	14.72
^{18}O+^{24}Mg	1.1	96	8.68	15.93	-1.27	14.65
^{16}O+^{28}Si	1	112	8.63	18.69	-1.51	17.18
^{16}O+^{29}Si	1.045	112	8.69	18.56	-1.49	17.07
^{16}O+^{30}Si	1.090	112	8.75	18.42	-1.46	16.96
^{18}O+^{28}Si	1.090	112	8.81	18.31	-1.45	16.86
^{24}Mg+^{32}S	1	192	9.03	30.61	-2.43	28.18
^{24}Mg+^{34}S	1.071	192	9.14	30.25	-2.37	27.88
^{26}Mg+^{32}S	1.071	192	9.17	30.14	-2.34	27.80
^{26}Mg+^{34}S	1.143	192	9.28	29.79	-2.29	27.50
^{28}Si+^{28}Si	1	196	9.04	31.22	-2.48	28.74
^{28}Si+^{30}Si	1.071	196	9.16	30.81	-2.41	28.40
^{30}Si+^{30}Si	1.143	196	9.29	30.38	-2.32	28.06
^{28}Si+^{58}Ni	1.048	392	9.79	57.66	-4.44	53.22
^{28}Si+^{62}Ni	1.143	392	9.94	56.79	-4.27	52.52
^{28}Si+^{64}Ni	1.190	392	10.01	56.40	-4.20	52.19
^{30}Si+^{58}Ni	1.095	392	9.92	56.91	-4.29	52.62
^{30}Si+^{62}Ni	1.190	392	10.07	56.06	-4.12	51.94
^{30}Si+^{64}Ni	1.238	392	10.14	56.68	-4.06	51.61

Table 2. (Continued)

Reaction	N/Z	Z_1Z_2	R_B	V_C	V_N	V_B
^{40}Ca+^{40}Ca	1	400	9.68	59.51	-4.63	54.88
^{40}Ca+^{44}Ca	1.1	400	9.87	58.36	-4.43	53.93
^{40}Ca+^{48}Ca	1.2	400	10.05	57.32	-4.24	53.08
^{48}Ca+^{48}Ca	1.4	400	10.42	55.28	-3.88	51.40
^{40}Ca+^{46}Ti	1.048	440	9.86	64.26	-4.96	59.30
^{40}Ca+^{48}Ti	1.095	440	9.95	63.69	-4.85	58.84
^{40}Ca+^{50}Ti	1.143	440	10.04	63.12	-4.72	58.40
^{32}S+^{58}Ni	1.045	448	9.90	65.17	-5.02	60.15
^{32}S+^{64}Ni	1.182	448	10.12	63.76	-4.76	59.00
^{34}S+^{58}Ni	1.090	448	10.02	64.39	-4.86	59.53
^{34}S+^{64}Ni	1.227	448	10.24	63.01	-4.60	58.41
^{36}S+^{58}Ni	1.136	448	10.13	63.69	-4.73	58.96
^{36}S+^{64}Ni	1.273	448	10.35	62.33	-4.48	57.85
^{40}Ar+^{58}Ni	1.130	504	10.21	71.09	-5.33	65.76
^{40}Ar+^{60}Ni	1.174	504	10.29	70.54	-5.20	65.34
^{40}Ar+^{62}Ni	1.217	504	10.36	70.05	-5.13	64.93
^{40}Ar+^{64}Ni	1.260	504	10.43	69.60	-5.06	64.54
^{40}Ca+^{58}Ni	1.042	560	10.10	79.85	-6.15	73.70
^{40}Ca+^{62}Ni	1.125	560	10.25	78.69	-5.93	72.76
^{48}Ti+^{58}Ni	1.12	616	10.37	85.55	-6.45	79.30
^{48}Ti+^{60}Ni	1.16	616	10.45	84.90	-6.30	78.84
^{48}Ti+^{64}Ni	1.24	616	10.59	83.77	-6.13	77.97
^{46}Ti+^{64}Ni	1.2	616	10.50	84.49	-6.27	78.49
^{50}Ti+^{60}Ni	1.2	616	10.54	84.16	-6.14	78.32
^{58}Ni+^{58}Ni	1.071	784	10.51	107.43	-8.25	99.18
^{58}Ni+^{64}Ni	1.178	784	10.74	105.14	-7.77	97.36
^{64}Ni+^{64}Ni	1.286	784	10.96	103.02	-7.41	95.61

Table 3. The calculated barrier positions R_B and heights V_B for different fusion reactions using Prox. DP potential. The nuclear and Coulomb potentials in $r = R_B$ have also been reported. The systems are listed with respect to their increasing Z_1Z_2 values.

Reaction	N/Z	Z_1Z_2	R_B	V_C	V_N	V_B
^{12}C+^{28}Si	1	84	8.36	14.46	-1.31	13.15
^{12}C+^{29}Si	1.05	84	8.43	14.34	-1.30	13.04
^{12}C+^{30}Si	1.1	84	8.50	14.22	-1.30	12.92
^{16}O+^{24}Mg	1	96	8.37	16.51	-1.50	15.01
^{16}O+^{26}Mg	1.1	96	8.53	16.20	-1.48	14.72
^{18}O+^{24}Mg	1.1	96	8.60	16.07	-1.47	14.60
^{16}O+^{28}Si	1	112	8.48	19.01	-1.72	17.29
^{16}O+^{29}Si	1.045	112	8.56	18.83	-1.69	17.14
^{16}O+^{30}Si	1.090	112	8.63	18.68	-1.68	17.00
^{18}O+^{28}Si	1.090	112	8.72	18.48	-1.66	16.82
^{24}Mg+^{32}S	1	192	8.84	31.27	-2.76	28.51
^{24}Mg+^{34}S	1.071	192	8.98	30.78	-2.68	28.10
^{26}Mg+^{32}S	1.071	192	9.02	30.65	-2.66	27.99
^{26}Mg+^{34}S	1.143	192	9.16	30.18	-2.58	27.60
^{28}Si+^{28}Si	1	196	8.85	31.89	-2.80	29.08
^{28}Si+^{30}Si	1.071	196	9.00	31.35	-2.74	28.61
^{30}Si+^{30}Si	1.143	196	9.16	30.81	-2.64	28.17
^{28}Si+^{58}Ni	1.048	392	9.62	58.67	-4.73	53.94
^{28}Si+^{62}Ni	1.143	392	9.78	57.71	-4.57	53.14
^{28}Si+^{64}Ni	1.190	392	9.85	57.30	-4.52	52.78
^{30}Si+^{58}Ni	1.095	392	9.78	57.71	-4.57	53.14
^{30}Si+^{62}Ni	1.190	392	9.94	56.78	-4.41	52.37
^{30}Si+^{64}Ni	1.238	392	10.01	56.39	-4.37	52.01

Table 3. (Continued)

Reaction	N/Z	Z_1Z_2	R_B	V_C	V_N	V_B
^{40}Ca+^{40}Ca	1	400	9.50	60.62	-4.95	55.67
^{40}Ca+^{44}Ca	1.1	400	9.72	59.25	-4.74	54.51
^{40}Ca+^{48}Ca	1.2	400	9.92	58.05	-4.54	53.51
^{48}Ca+^{48}Ca	1.4	400	10.33	55.75	-4.23	51.52
^{40}Ca+^{46}Ti	1.048	440	9.70	65.31	-5.24	60.07
^{40}Ca+^{48}Ti	1.095	440	9.80	64.64	-5.13	59.51
^{40}Ca+^{50}Ti	1.143	440	9.90	64.00	-5.00	59.00
^{32}S+^{58}Ni	1.045	448	9.74	66.23	-5.25	60.97
^{32}S+^{64}Ni	1.182	448	9.97	64.69	-5.02	59.67
^{34}S+^{58}Ni	1.090	448	9.88	65.29	-5.10	60.18
^{34}S+^{64}Ni	1.227	448	10.11	63.80	-4.88	58.92
^{36}S+^{58}Ni	1.136	448	10.01	64.44	-4.97	59.47
^{36}S+^{64}Ni	1.273	448	10.24	62.99	-4.76	58.23
^{40}Ar+^{58}Ni	1.130	504	10.08	71.99	-5.59	66.40
^{40}Ar+^{60}Ni	1.174	504	10.17	71.35	-5.43	65.92
^{40}Ar+^{62}Ni	1.217	504	10.24	70.87	-5.40	65.47
^{40}Ar+^{64}Ni	1.260	504	10.32	70.31	-5.28	65.03
^{40}Ca+^{58}Ni	1.042	560	9.93	81.20	-6.46	74.74
^{40}Ca+^{62}Ni	1.125	560	10.09	79.91	-6.24	73.67
^{48}Ti+^{58}Ni	1.12	616	10.23	86.70	-6.70	80.000
^{48}Ti+^{60}Ni	1.16	616	10.31	86.03	-6.60	79.43
^{48}Ti+^{64}Ni	1.24	616	10.47	84.71	-6.34	78.37
^{46}Ti+^{64}Ni	1.2	616	10.37	85.53	-6.47	79.06
^{50}Ti+^{60}Ni	1.2	616	10.41	85.20	-6.43	78.77
^{58}Ni+^{58}Ni	1.071	784	10.34	109.17	-8.62	100.55
^{58}Ni+^{64}Ni	1.178	784	10.59	106.60	-8.08	98.52
^{64}Ni+^{64}Ni	1.286	784	10.83	104.24	-7.67	96.57

Table 4. The calculated barrier positions R_B and heights V_B for different fusion reactions using Prox. 2010 potential. The nuclear and Coulomb potentials in $r = R_B$ have also been reported. The systems are listed with respect to their increasing Z_1Z_2 values.

Reaction	N/Z	Z_1Z_2	R_B	V_C	V_N	V_B
^{12}C+^{28}Si	1	84	8.29	14.58	-1.32	13.26
^{12}C+^{29}Si	1.05	84	8.35	14.48	-1.30	13.18
^{12}C+^{30}Si	1.1	84	8.41	14.37	-1.27	13.10
^{16}O+^{24}Mg	1	96	8.34	16.52	-1.48	15.08
^{16}O+^{26}Mg	1.1	96	8.47	16.32	-1.44	14.88
^{18}O+^{24}Mg	1.1	96	8.52	16.22	-1.42	14.80
^{16}O+^{28}Si	1	112	8.46	19.05	-1.69	17.36
^{16}O+^{29}Si	1.045	112	8.52	18.92	-1.67	17.25
^{16}O+^{30}Si	1.090	112	8.58	18.79	-1.64	17.15
^{18}O+^{28}Si	1.090	112	8.64	18.65	-1.62	17.03
^{24}Mg+^{32}S	1	192	8.88	31.13	-2.62	28.5
^{24}Mg+^{34}S	1.071	192	8.99	30.75	-2.55	28.20
^{26}Mg+^{32}S	1.071	192	9.01	30.68	-2.56	28.12
^{26}Mg+^{34}S	1.143	192	9.11	30.34	-2.50	27.84
^{28}Si+^{28}Si	1	196	8.89	31.74	-2.67	29.07
^{28}Si+^{30}Si	1.071	196	9.01	31.31	-2.59	28.72
^{30}Si+^{30}Si	1.143	196	9.12	30.44	-2.53	28.41
^{28}Si+^{58}Ni	1.048	392	9.68	58.30	-4.49	53.81
^{28}Si+^{62}Ni	1.143	392	9.80	57.59	-4.43	53.16
^{28}Si+^{64}Ni	1.190	392	9.86	57.24	-4.36	52.88
^{30}Si+^{58}Ni	1.095	392	9.79	57.65	-4.43	53.22
^{30}Si+^{62}Ni	1.190	392	9.92	56.89	-4.28	52.61
^{30}Si+^{64}Ni	1.238	392	9.97	56.61	-4.26	52.35

Table 4. (Continued)

Reaction	N/Z	Z_1Z_2	R_B	V_C	V_N	V_B
^{40}Ca+^{40}Ca	1	400	9.57	60.18	-4.70	55.48
^{40}Ca+^{44}Ca	1.1	400	9.75	59.07	-4.52	54.55
^{40}Ca+^{48}Ca	1.2	400	9.90	58.17	-4.39	53.78
^{48}Ca+^{48}Ca	1.4	400	10.18	56.57	-4.17	52.40
^{40}Ca+^{46}Ti	1.048	440	9.76	64.91	-4.96	59.95
^{40}Ca+^{48}Ti	1.095	440	9.84	64.38	-4.88	59.50
^{40}Ca+^{50}Ti	1.143	440	9.91	63.92	-4.83	59.09
^{32}S+^{58}Ni	1.045	448	9.80	65.82	-5.02	60.08
^{32}S+^{64}Ni	1.182	448	9.99	64.57	-4.82	59.75
^{34}S+^{58}Ni	1.090	448	9.90	65.16	-4.96	60.20
^{34}S+^{64}Ni	1.227	448	10.08	63.99	-4.78	59.21
^{36}S+^{58}Ni	1.136	448	10.00	64.50	-4.85	59.65
^{36}S+^{64}Ni	1.273	448	10.18	63.36	-4.64	58.72
^{40}Ar+^{58}Ni	1.130	504	10.10	71.85	-5.34	66.51
^{40}Ar+^{60}Ni	1.174	504	10.16	71.43	-5.29	66.14
^{40}Ar+^{62}Ni	1.217	504	10.22	71.01	-5.22	65.79
^{40}Ar+^{64}Ni	1.260	504	10.28	70.59	-5.13	65.46
^{40}Ca+^{58}Ni	1.042	560	10.02	80.47	-6.02	74.45
^{40}Ca+^{62}Ni	1.125	560	10.15	79.44	-5.88	73.56
^{48}Ti+^{58}Ni	1.12	616	10.29	86.20	-6.25	79.95
^{48}Ti+^{60}Ni	1.16	616	10.35	85.69	-6.20	79.49
^{48}Ti+^{64}Ni	1.24	616	10.47	84.71	-6.04	78.67
^{46}Ti+^{64}Ni	1.2	616	10.39	85.37	-6.18	79.19
^{50}Ti+^{60}Ni	1.2	616	10.42	85.12	-6.14	78.98
^{58}Ni+^{58}Ni	1.071	784	10.47	107.82	-7.74	100.08
^{58}Ni+^{64}Ni	1.178	784	10.66	105.90	-7.48	98.42
^{64}Ni+^{64}Ni	1.286	784	10.84	104.13	-7.21	96.92

Table 5. The calculated values for fitting parameters α, β, γ and c, which are based on the Eqs. (14), (15), (16) and (20), respectively, for AW 95, Bass 80, Prox. DP and Prox. 2010 potentials.

Proximity-type potential	α	β	γ	c($E^0_{c.m.}$=1.125)	c($E^0_{c.m.}$=1.375)
AW 95	16.18	-14.31	31.45	155.83	73.57
Bass 80	18.26	-15.33	41.82	170.21	80.02
Prox. DP	20.78	-18.11	38.56	192.58	94.06
Prox. 2010	16.57	-13.63	28.80	146.33	69.78

Figure 1:

Figure 2:

Figure 3:

Figure 4:

Figure 5:

Figure 6:

Figure 7:

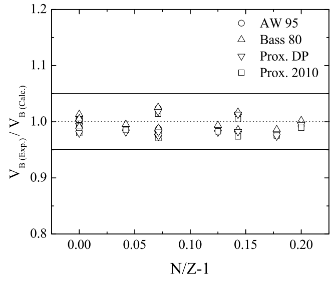
1.2
1.1
1.0
0.9
0.8
$V_{B\,(Exp.)} / V_{B\,(Calc.)}$
0.00
0.05
0.10
0.15
0.20
N/Z-1
AW 95
Bass 80
Prox. DP
Prox. 2010

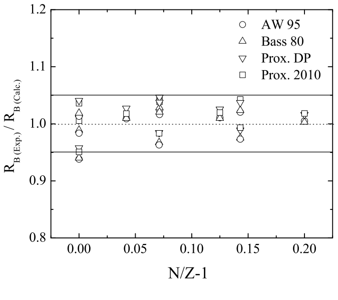
1.2
1.1
1.0
0.9
0.8
$R_{B\,(Exp.)} / R_{B\,(Calc.)}$
0.00
0.05
0.10
0.15
0.20
N/Z-1
AW 95
Bass 80
Prox. DP
Prox. 2010

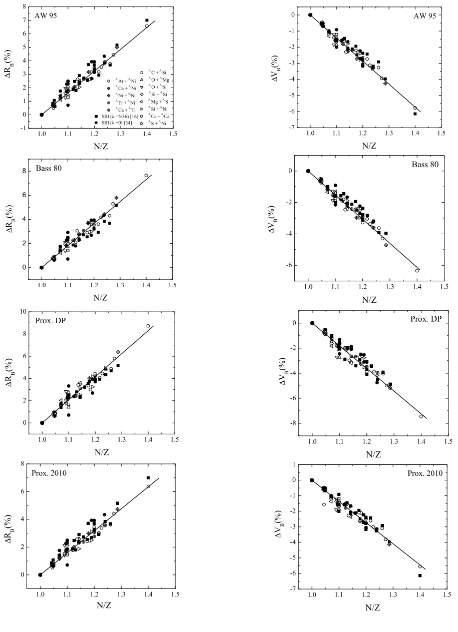
AW 95
Bass 80
Prox. DP
Prox. 2010
ΔR_B(%)
ΔV_B(%)
N/Z
^{A}Ar + ^{A}Ni
^{A}Ca + ^{A}Ni
^{A}Ni + ^{A}Ni
^{A}Ti + ^{A}Ni
^{A}Ca + ^{A}Ti
SIII (λ =5/36) [16]
SIII (λ =0) [34]
^{A}C + ^{A}Si
^{A}O + ^{A}Mg
^{A}O + ^{A}Si
^{A}Si + ^{A}Si
^{A}Mg + ^{A}S
^{A}Si + ^{A}Ni
^{A}Ca + ^{A}Ca
^{A}S + ^{A}Ni

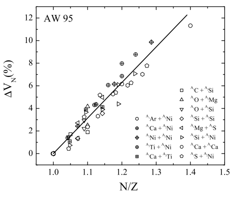
AW 95
$\Delta V_N(\%)$
12
10
8
6
4
2
0
1.0
1.1
1.2
1.3
1.4
1.5
N/Z
^{A}Ar + ^{A}Ni
^{A}Ca + ^{A}Ni
^{A}Ni + ^{A}Ni
^{A}Ti + ^{A}Ni
^{A}Ca + ^{A}Ti
^{A}C + ^{A}Si
^{A}O + ^{A}Mg
^{A}O + ^{A}Si
^{A}Si + ^{A}Si
^{A}Mg + ^{A}S
^{A}Si + ^{A}Ni
^{A}Ca + ^{A}Ca
^{A}S + ^{A}Ni

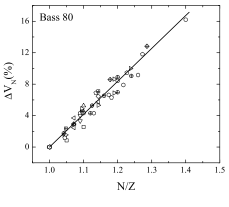
Bass 80
$\Delta V_N(\%)$
16
12
8
4
0
1.0
1.1
1.2
1.3
1.4
1.5
N/Z

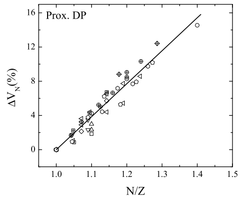
Prox. DP
$\Delta V_N(\%)$
16
12
8
4
0
1.0
1.1
1.2
1.3
1.4
1.5
N/Z

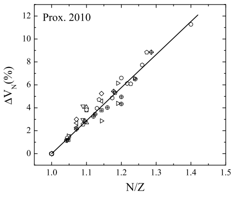
Prox. 2010
$\Delta V_N(\%)$
12
10
8
6
4
2
0
1.0
1.1
1.2
1.3
1.4
1.5
N/Z

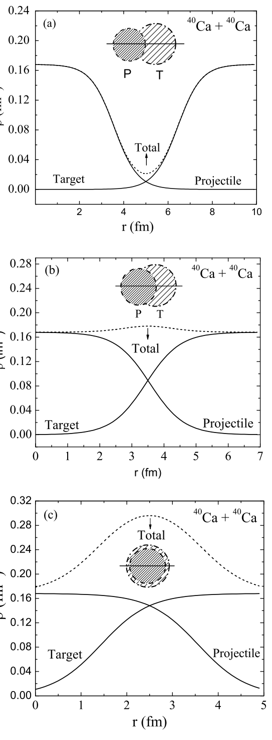
(a)
^{40}Ca + ^{40}Ca
P
T
Total
Target
Projectile
ρ (fm^{-3})
r (fm)
0.24
0.20
0.16
0.12
0.08
0.04
0.00
2
4
6
8
10
(b)
^{40}Ca + ^{40}Ca
P
T
Total
Target
Projectile
ρ (fm^{-3})
r (fm)
0.28
0.24
0.20
0.16
0.12
0.08
0.04
0.00
0
1
2
3
4
5
6
7
(c)
^{40}Ca + ^{40}Ca
Total
Target
Projectile
ρ (fm^{-3})
r (fm)
0.32
0.28
0.24
0.20
0.16
0.12
0.08
0.04
0.00
0
1
2
3
4
5

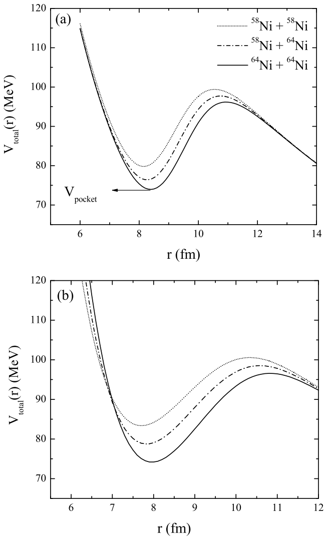
(a)
^{58}Ni + ^{58}Ni
^{58}Ni + ^{64}Ni
^{64}Ni + ^{64}Ni
V_{pocket}
$V_{total}(r)$ (MeV)
r (fm)
120
110
100
90
80
70
6
8
10
12
14
(b)
$V_{total}(r)$ (MeV)
r (fm)
120
110
100
90
80
70
6
7
8
9
10
11
12

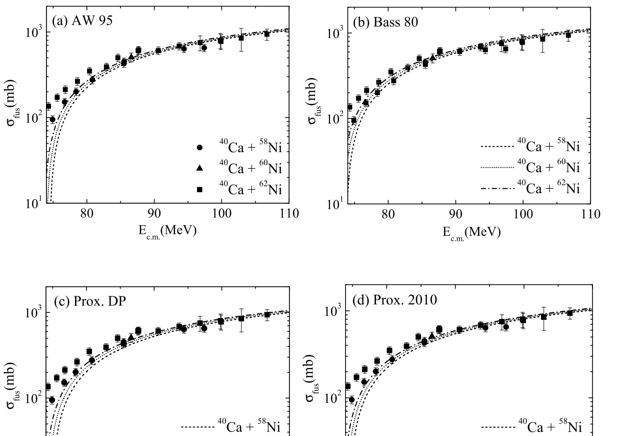
(a) AW 95
(b) Bass 80
(c) Prox. DP
(d) Prox. 2010
σ_{fus}(mb)
$E_{c.m.}$(MeV)
10^1
10^2
10^3
80
90
100
110
● ^{40}Ca + ^{58}Ni
▲ ^{40}Ca + ^{60}Ni
■ ^{40}Ca + ^{62}Ni
^{40}Ca + ^{58}Ni
^{40}Ca + ^{60}Ni
^{40}Ca + ^{62}Ni

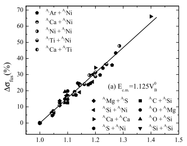
^{A_1}Ar + ^{A_2}Ni
^{A_1}Ca + ^{A_2}Ni
^{A_1}Ni + ^{A_2}Ni
^{A_1}Ti + ^{A_2}Ni
^{A_1}Ca + ^{A_2}Ti
(a) $E_{c.m.}$=1.125V_B^0
^{A_1}Mg + ^{A_2}S
^{A_1}Si + ^{A_2}Ni
^{A_1}Ca + ^{A_2}Ca
^{A_1}S + ^{A_2}Ni
^{A_1}C + ^{A_2}Si
^{A_1}O + ^{A_2}Mg
^{A_1}O + ^{A_2}Si
^{A_1}Si + ^{A_2}Si
$\Delta\sigma_{fus}$(%)
N/Z
0
10
20
30
40
50
60
70
1.0
1.1
1.2
1.3
1.4
1.5

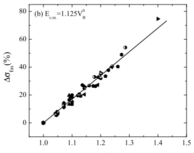
(b) $E_{c.m.}$=1.125V_B^0
$\Delta\sigma_{fus}$(%)
N/Z
0
20
40
60
80
1.0
1.1
1.2
1.3
1.4
1.5

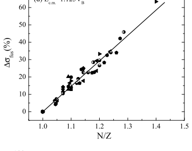
(d) $E_{c.m.}$=1.125V_B^0
$\Delta\sigma_{fus}$(%)
N/Z
0
10
20
30
40
50
60
70
1.0
1.1
1.2
1.3
1.4
1.5

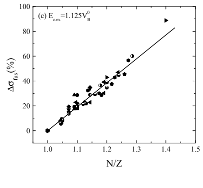
(c) $E_{c.m.}$=1.125V_B^0
$\Delta\sigma_{fus}$(%)
N/Z
0
20
40
60
80
100
1.0
1.1
1.2
1.3
1.4
1.5

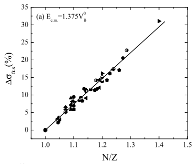
(a) $E_{c.m.}$=1.375V_B^0
$\Delta\sigma_{fus}$(%)
N/Z
0
5
10
15
20
25
30
35
1.0
1.1
1.2
1.3
1.4
1.5

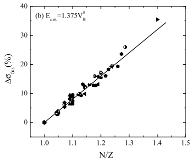
(b) $E_{c.m.}$=1.375V_B^0
$\Delta\sigma_{fus}$(%)
N/Z
0
10
20
30
40
1.0
1.1
1.2
1.3
1.4
1.5

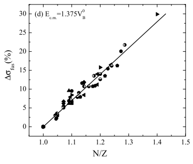
(d) $E_{c.m.}$=1.375V_B^0
$\Delta\sigma_{fus}$(%)
N/Z
0
5
10
15
20
25
30
1.0
1.1
1.2
1.3
1.4
1.5

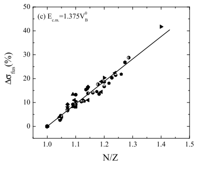
(c) $E_{c.m.}$=1.375V_B^0
$\Delta\sigma_{fus}$(%)
N/Z
0
10
20
30
40
50
1.0
1.1
1.2
1.3
1.4
1.5